DEVELOPMENT OF THE FHR ADVANCED NATURAL CIRCULATION ANALYSIS (FANCY) CODE

Z. Guo[1,2], N. Zweibaum[1], M. Shao[3], L. R. Huddar[1], P. F. Peterson[1], S. Qiu[2]
[1]: Department of Nuclear Engineering, University of California, Berkeley, 4118 Etcheverry Hall, Berkeley, CA 94720, USA
[2]: Department of Nuclear Science and Technology, Xi'an Jiaotong University, Xi'an, 710049, China
[3]: Lawrence Berkeley National Laboratory, Berkeley, CA 94720, USA
zhangpengguo@berkeley.edu; nicolas.zweibaum@berkeley.edu; myshao@lbl.gov; lakshana.huddar@berkeley.edu; peterson@nuc.berkeley.edu; szqiu@mail.xjtu.edu.cn

ABSTRACT

The University of California, Berkeley (UCB) is performing thermal hydraulics safety analysis to develop the technical basis for design and licensing of fluoride-salt-cooled, high-temperature reactors (FHRs). FHR designs investigated by UCB use natural circulation for emergency, passive decay heat removal when normal decay heat removal systems fail. The FHR advanced natural circulation analysis (FANCY) code has been developed for assessment of passive decay heat removal capability and safety analysis of these innovative system designs. The FANCY code uses a one-dimensional, semi-implicit scheme to solve for pressure-linked mass, momentum and energy conservation equations. Graph theory is used to automatically generate a staggered mesh for complicated pipe network systems. Heat structure models have been implemented for three types of boundary conditions (Dirichlet, Neumann and Robin boundary conditions). Heat structures can be composed of several layers of different materials, and are used for simulation of heat structure temperature distribution and heat transfer rate. Control models are used to simulate sequences of events or trips of safety systems. A proportional-integral controller is also used to automatically make thermal hydraulic systems reach desired steady state conditions. A point kinetics model is used to model reactor kinetics behavior with temperature reactivity feedback. The underlying large sparse linear systems in these models are efficiently solved by using direct and iterative solvers provided by the SuperLU code on high performance machines. Input interfaces are designed to increase the flexibility of simulation for complicated thermal hydraulic systems. Detailed code-to-code comparison with established thermal hydraulic system codes such as RELAP5, and validation against experimental data from UCB's Compact Integral Effects Test facility, are performed in a companion paper. This paper mainly focuses on the methodology used to develop the FANCY code, and safety analysis of the Mark 1 pebble-bed FHR under development at UCB is performed.

KEYWORDS
FHR, natural circulation, code methodology

1. INTRODUCTION

The University of California, Berkeley (UCB) is developing methods to design and perform safety analysis for fluoride-salt-cooled, high-temperature reactors (FHRs) in collaboration with

the Massachusetts Institute of Technology and University of Wisconsin [1]. Flibe is the baseline coolant for FHRs, while Dowtherm A, a heat transfer oil, has been identified as an appropriate simulant fluid for scaled heat transfer experiments for FHRs [2]. FHRs have inherently safe features, such as natural-circulation-driven systems to passively remove decay heat from the reactor core during design basis and beyond design basis accidents. UCB has developed a commercial design for a small modular FHR, the Mark 1 (Mk1) pebble-bed FHR (PB-FHR) [3]. The capability to perform steady-state and transient system analysis is a key issue for licensing new reactor designs. Best-estimate system codes play a key role in the licensing of nuclear technology because of the impracticality of executing full-scale safety-related experiments. However, current nuclear commercial codes, such as RELAP5-3D and Flownex, have mainly been developed for light water reactors, which require the use of comprehensive two-phase flow models. This capability is not required to simulate single-phase flow phenomena in FHRs, whose baseline coolant, flibe, remains liquid up to 1430°C at atmospheric pressure. The FHR advanced natural circulation analysis (FANCY) code has been developed specifically for FHR technology modeling [4]. It has the capability to model the Mk1 PB-FHR power plant system behavior under steady state and transient conditions. FANCY has a modular structure, which makes it easy to be maintained and updated. Physical models can easily be modified and added to the code for specific FHR problems, sensitivity studies and uncertainty analysis. Verification and validation (V&V) of the FANCY code is being performed, including detailed code-to-code comparison with established thermal hydraulic system codes such as RELAP5-3D and Flownex, and validation against experimental data from UCB's Compact Integral Effects Test (CIET) facility [5, 6]. These efforts are detailed in a companion paper [7]. The current paper mainly focuses on the development methodology of the FANCY code and on preliminary safety analysis results for the Mk1 PB-FHR that is based on equivalent model, including two kinds of anticipated transient without scram (ATWS), such as loss of force circulation (LOFC) and loss of heat sink (LOHS).

2. SYSTEM CODE MODEL

This chapter briefly describes the mathematic models of the FANCY code, which mainly includes the hydrodynamic model, heat structure model, coupled strategy model, closure model, reactor kinetic model, system control model, sparse matrix solve model.

2.1 Hydrodynamic model

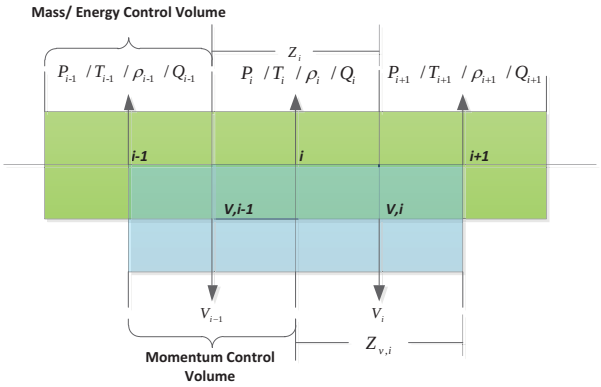

Figure 1. Staggered mesh method schematic

The fluid governing equations in each CV that are based on integral balance laws implemented in the code are derived from the Navier–Stokes equations. These space and time averaging models are widely used in safety analysis codes for nuclear systems. They neglect the effects of small scale processes on macroscopic steady or transient phenomena. This assumption is compensated by the use of suitable closure models for friction factor and heat transfer coefficients, which are usually found from separate effect tests.

As shown in Fig. 1, in order to avoid odd-even decoupling between pressure and velocity , a staggered mesh method is used [8]. On a staggered grid, the scalar variables (pressure, density, total enthalpy, etc.) are stored in the cell centers of the control volumes, whereas the vector variables (velocity or momentum) are located at the cell faces. As a result, the main control volume and momentum control volume are obtained separately. This is different from a collocated grid arrangement, where all variables are stored in the same position. Staggered storage schemes are mainly used for structured grids for compressible or incompressible flow simulations. The hydrodynamic component can be classified as a general component without branches, such as pipe, reactor core channel, primary side or secondary side of a heat exchanger, or pump. If the system has additional branches like T-junctions, cross junctions, or multiple junctions, a specific branch model will be used.

After integration of the Navier–Stokes equations, the macroscopic mass, momentum, and energy governing equations are obtained on the staggered mesh. The finite volume scheme with first order upwind method, combined with time discretization using a semi-implicit scheme, are used to obtain the differential forms of the conservation equations, as shown in Eq. (1) – (4):

Mass conservation equation:

$$A_i \frac{\rho_i^{n+1} - \rho_i^n}{\Delta t} + \frac{\rho_{v,i}^n u_{v,i}^{n+1} A_{v,i} - \rho_{v,i-1}^n u_{v,i-1}^{n+1} A_{v,i-1}}{Z_i} = 0 \tag{1}$$

Momentum conservation equation:

$$\begin{aligned} & A_{v,i} \frac{\rho_{v,i}^n u_{v,i}^{n+1} - \rho_{v,i}^n u_{v,i}^n}{\Delta t} + \frac{\rho_{i+1}^n \left(u_{i+1}^n\right)^2 A_{i+1} - \rho_i^n \left(u_i^n\right)^2 A_i}{Z_{v,i}} \\ & = -\frac{P_{i+1}^{n+1} A_{i+1} - P_i^{n+1} A_i}{Z_{v,i}} - \rho_{v,i}^n g A_{v,i} \sin\theta + \frac{\Delta P_{pump}}{Z_{v,i}} - \frac{1}{2D_{v,i}} \left(f_i + \frac{K}{Z_{v,i}}\right) \rho_{v,i}^n \left|u_{v,i}^n\right| u_{v,i}^n A_{v,i} \end{aligned} \tag{2}$$

Energy conservation equation:

$$V_i[\rho_i^n \frac{H_i^{n+1} - H_i^n}{\Delta t} + H_i^n \frac{\rho_i^{n+1} - \rho_i^n}{\Delta t}] + (\rho H)_{v,i}^n u_{v,i}^{n+1} A_{v,i} - (\rho H)_{v,i-1}^n u_{v,i-1}^{n+1} A_{v,i-1} = Q_i \tag{3}$$

Coolant state equation:

$$\frac{\rho_i^{n+1} - \rho_i^n}{\Delta t} = \frac{\partial \rho(p,H)_i^n}{\partial H} \frac{H_i^{n+1} - H_i^n}{\Delta t} + \frac{\partial \rho(p,H)_i^n}{\partial p} \frac{p_i^{n+1} - p_i^n}{\Delta t} \tag{4}$$

The pump head is added to the momentum model to simulate forced circulation. Although the fluid is assumed to be incompressible, the mass conservation equation considers the effect of thermal expansion by including the density derivative term with respect to time. Wall friction forces are neglected in the energy equation, so no dissipation rate is considered in the energy model. Because fluid density is independent of pressure for the single-phase, incompressible molten salt, the partial derivative of density with respect to pressure is also neglected.

The fluid mass, energy and momentum equations are coupled and then reduced to a pressure equation in one momentum CV. A linear system of equations is obtained, which can be further reduced to N linear equations for pressure, as shown in Eq. (5).

$$A\begin{bmatrix} \Delta P_1 \\ \vdots \\ \Delta P_{i-1} \\ \Delta P_i \\ \Delta P_{i+1} \\ \vdots \\ \Delta P_N \end{bmatrix} = B \tag{5}$$

N is the total number of CVs , A is an $N \times N$ sparse matrix, and B is an N -dimensional vector. A and B are determined by the previous time step value. The non-zero elements in the matrix reflect the relationships between pressures among the main CVs, and upstream and downstream neighboring CVs. The sparse matrix is solved at each time step to get a new pressure distribution. Updated flow velocities and thermal properties are obtained from the new pressure distribution at each time step.

Each leg of branch is characterized by individual form loss coefficient. Since branches can have multiple inlets and outlets, the mass and energy equations for the branch model contains more than one advection term in governing equations.

For a staggered mesh, an appropriate interpolation model must also be considered. The first order upwind method is employed to avoid numerical oscillation Eq. (6) [8], where ϕ means thermal properties. The thermal properties of the momentum CV are updated based on the velocity direction.

$$u_i \phi_{v,i} = \phi_{i-1} \max\{u_i, 0\} - \phi_i \max\{-u_i, 0\} \tag{6}$$

Special attention should be paid on the angle interpolation for momentum CV which is a junction that connects two adjacent main CVs. Using a simple linear interpolation may introduce additional driving forces or resistances in the loop, which will cause significant distortions and increase uncertainty in code results when modeling natural circulation, where mass flow rates are usually small.

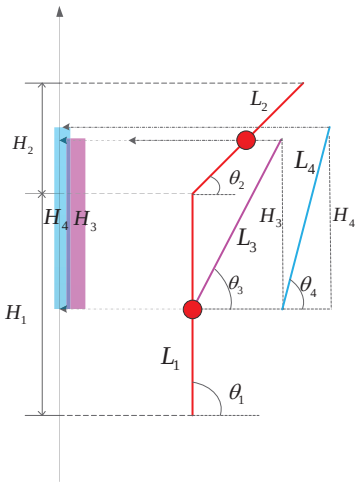

Figure 2. Angle interpolation for momentum CV in staggered mesh

Fig. 2 shows a simple method to get the angle of a junction (momentum CV) between pipes main CVs is to use a simple linear interpolation, $\theta_4 = (\theta_1 + \theta_2)/2$. However, if we use angle θ_4 to derive pipe elevation, the resulting effective height, H_4 is larger than the real height H_3, leading to higher hydrostatic pressure. Instead, it is better to use a more accurate angle interpolation θ_3 (Eq. (7)).

$$\theta_3 = \arcsin\left[\frac{H_3}{L_3}\right] = \arcsin\left[\frac{L_1 \sin\theta_1/2 + L_2 \sin\theta_2/2}{(L_1 + L_2)/2}\right] \tag{7}$$

Because θ_3 is calculated from the actual effective height, no artificial driving force or resistance is introduced.

2.2 Staggered mesh generation model

For a large disperse region like a pipe network, mesh generation is harder to implement, especially when there are multiple connected or disconnected loops. Graph theory is used to generate, organize and store a staggered mesh of complicated pipe networks in disperse region. Basic information for hydrodynamic components, including pipes and branches, as well as their relationships are then defined, and an element-node (branch-node) incidence matrix is generated following graph theory matrix pattern [9, 10].

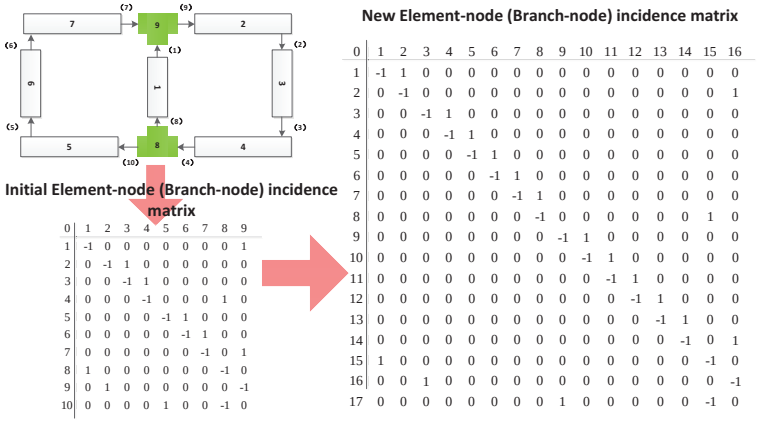

Figure 3. Simple hydrodynamic system (left) with corresponding incidence matrix (right)

Fig. 3 shows a simple hydrodynamic system with two individual loops connected by two branches, and only one main CV in each hydrodynamic component. This system is represented by an $n \times m$ incidence matrix $A = (a_{ij})$. Each row of the matrix is a junction index and each column is a hydrodynamic component index. $a_{ij} = 1$ if junction *i* connects *to* component *j*, $a_{ij} = -1$ if junction *i* connects *from* component *j*, and $a_{ij} = 0$ if junction *i* is not adjacent to component *j*. The corresponding small incidence matrix is generated from relationships between hydraulic components, derived from input information. Furthermore, each hydraulics component can be sub-divided into more than one CV to obtain a mesh-independent solution [11].

Consequently, a new element-node (branch-node) incidence matrix is automatically generated based on the actual number of CVs in each component.

Moreover, some characteristics of the incidence matrix can be used to check whether mesh generation is logical or not. First, the ∞-norm of the matrix must be equal to 2, and the row sum of matrix must be equal to zero, since each junction (momentum CV) only connects to two adjacent main CVs (mass/energy CVs). The 1-norm of the matrix must be greater than or equal to 2. Besides,the new element-node (branch-node) incidence matrix is useful to generate the adjacency matrix and tree for directed graph, which are necessary to set up initial conditions and check whether the hydraulic loop is closed.

2.3 Heat structure model

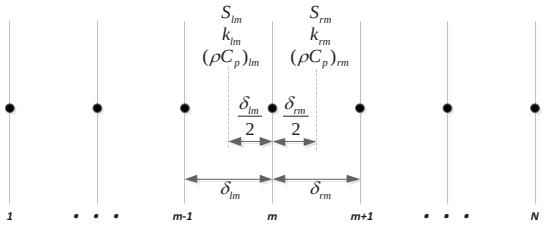

Figure 4. Mesh points for heat structure

The heat structure model is added to the code for simulation of heat transfer into and across solid boundaries of hydrodynamic volumes. Spatial finite difference approximation is used to obtain the finite differential form of the heat conduction equation. Fig. 4 shows the mesh point layout. Thermal properties at a CV interface can be derived from interpolation from neighboring mesh nodes. The fully implicit form of the finite difference approximation for the heat conduction model at internal mesh nodes is as follows:

$$(T_m^{n+1} - T_m^n)\frac{G_m}{\Delta t} = (T_{m-1}^{n+1} - T_m^{n+1})k_{lm}\delta_{lm}^s + (T_{m+1}^{n+1} - T_m^{n+1})k_{rm}\delta_{rm}^s + Q(\delta_{lm}^v + \delta_{rm}^v) \quad (8)$$

Where δ and G_m is the factors depending on geometry (rectangular, cylindrical and spherical geometries).

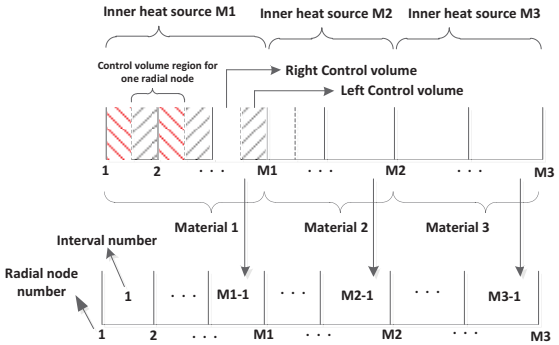

Figure 5. Inner heat source distribution and inner distance distribution

As is shown in Fig. 5 , the mesh of the heat structure model consists of different spacings (non-uniform mesh) , varying materials and different boundary conditions (Dirichlet, Neumann and Robin boundary conditions). There are fine mesh in regions where temperature gradients are large and coarse mesh in regions where temperature gradients are small. Besides, any radial node can be used as a boundary point to divide varying materials or heat sources in the mesh. The model automatically calculates both the right and left CVs for each radial node and sums up the volumes to get the right power density within specific material layer intervals for different types of geometry.

2.4 Closure models

The closure models in FANCY comprise the thermophysical properties of the fluid, friction factors and heat transfer coefficients. Thermophysical properties of Flibe and Dowtherm A have been added to FANCY so that scaled experimental loops using the simulant oil and FHR thermal hydraulics can be simulated. All fluid thermophysical properties depend on temperature and are independent of pressure for single-phase flow [12]. Thermophysical properties of stainless steel and copper—candidate materials for the FHR and scaled heat transfer loops using Dowtherm A—have also been included. For graphite in the pebble fuel, empirical correlations from AVR fuel are employed, which consider both temperature and fast neutron irradiation effects on fuel thermophysical properties [13]. Thermophysical properties of TRISO particles are independent of temperature [14].

The main friction factor and Nusselt number correlations are shown in Table I. The proper choice of semi-empirical correlations determines the accuracy of simulation results. The trend and distribution of temperatures during transients is mainly based on heat transfer coefficients. If the Nusselt number is lower, peak temperatures during transient scenarios will be higher. In order to conservatively estimate temperatures in the system and guarantee safety of the reactor, sensitivity studies for heat transfer coefficients are necessary.

Table I . Friction factor and Nusselt number correlation models

Component	Friction factor
Pipe, branch, heat transfer channel	$f_L = \frac{64}{\mathrm{Re}\,\phi_s} \; (0 \le \mathrm{Re} \le 2{,}200)$ [6]
	$f_{L,T} = (3.75 - \frac{8250}{\mathrm{Re}})(f_{T,3000} - f_{L,2200}) + f_{L,2200} \; (2{,}200 \le \mathrm{Re} \le 3{,}000)$ [6]
	$\frac{1}{\sqrt{f_T}} = -2\log_{10}(\frac{\varepsilon}{3.7D} + \frac{2.51}{\mathrm{Re}}[1.114 - 2\log_{10}(\frac{\varepsilon}{D} + \frac{21.25}{\mathrm{Re}^{0.9}})]) \; (\mathrm{Re} \ge 3000)$ [6]
Reactor core	$f = \frac{(1-\varepsilon)}{\varepsilon^3}\left(\frac{150(1-\varepsilon)}{\mathrm{Re}} + 1.75\right) \; (0.1 < \mathrm{Re}/(1-\varepsilon) < 500)$ [15]
Component	Nusselt number
Pipe, branch, heat transfer channel	Nu = 4.36 (laminar forced convection) [16]

$$Nu_L = \left\{ 0.825 + \frac{0.387(Ra_L)^{\frac{1}{6}}}{\left[1+(\frac{0.492}{\Pr})^{\frac{9}{16}}\right]^{\frac{8}{27}}} \right\}^2 = h_L \frac{L}{k}$$ (natural convection) [17]

$$Nu = 0.023 \mathrm{Re}^{0.8} \Pr^n = h\frac{D}{K}$$ (turbulent forced convection) [18]

Reactor core $Nu = 2 + 1.1 \Pr^{1/3} \mathrm{Re}^{0.6}$ (porous media) [19]

2.5 System control model

For safety analysis as well as risk analysis of the Mk1 PB-FHR and system simulation for the CIET loop, a sequence of events or actions is modeled. A control logic tree can be used to model system control and the decision making process based on Boolean algebra (Fig. 6). Besides, FANCY uses proportional and integral controls to make simulations converge faster under steady state.

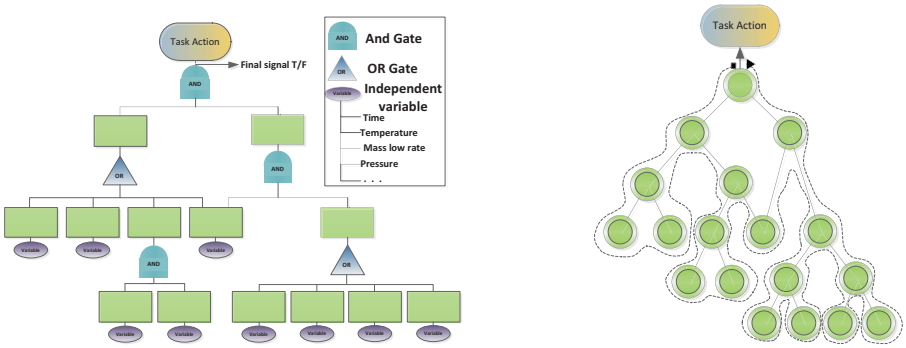

(a) Control logic tree (Boolean algebra) (b) Corresponding binary tree

Figure 6. Control logic tree for event sequences

2.6 Reactor kinetics model

The point kinetics model is used to obtain reactor power based on temperature reactivity feedback. This model is adequate when the spatial distribution of power can be assumed nearly constant. Due to the lack of neutronics experimental data for PB-FHRs, the kinetic parameters from gas-cooled reactors are employed [13]. The reactivity feedback model considers varying space effects, and the temperature feedback coefficients are obtained from MCNP5 calculations of the Mk1 PB-FHR core [20], as shown in Table II. Weight factors are used in the reactivity feedback model to take into account neutron worth at various locations in the reactor core.

Table II Temperature coefficients of reactivity for the Mk1 PB-FHR [20]

Component	Mk1 PB-FHR temperature reactivity coefficient (pcm/K)
Fuel	–3.8
Coolant	–1.8
Inner graphite reflector	+0.9
Graphite moderator	–0.7
Outer graphite reflector	+0.9

When the reactor is shut down and power is below 5% of nominal power, a specific decay heat curve for the Mk1 PB-FHR is employed, derived from three classes of isotopes in ORIGEN – actinides, fission and activation products [20].

2.7 Sparse matrix solver model

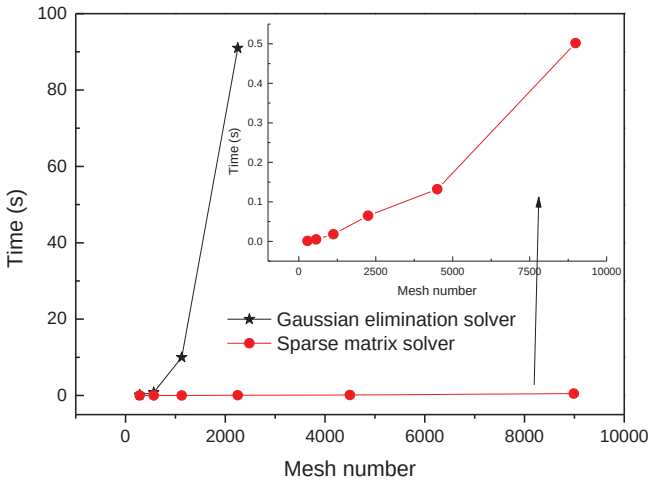

Figure 7. Performance comparison between Gaussian elimination solver and sparse matrix solver

The major computational work is to solve a sequence of linear systems at each time step.

$$A(t_i)x(t_i) = B(t_i)\ (i = 0,1,\cdots,L) \tag{9}$$

As the coefficient matrices are sparse, the generalized minimal residual (GMRES) method [21] with right preconditioning is used to solve these linear systems. Since *A(t)* and *B(t)* depend continuously on *t*, except when step changes happen in the system (e.g. pump coastdown, reactor power level change, valve opening or closing), the solution *x(t)* is also continuous. Therefore, $x(t_{i-1})$ serves as an initial guess for GMRES when solving $A(t_i)x(t_i) = B(t_i)\ (i = 0,1,\cdots,L)$. In addition, we propose the following preconditioning strategy for GMRES. Initially, $x(t_o) = A(t_o)^{-1}B(t_o)$ is solved using a sparse direct method based on sparse LU factorization [22]. Then, $A(t_o)^{-1}$ is used as the preconditioner for GMRES at subsequent time steps. If GMRES fails to converge after five iterations at time t_i, we compute $x(t_i)$ using the sparse

direct method, and replace the preconditioner by $A(t_i)^{-1}$. This strategy adaptively updates the preconditioner when it deteriorates, ensuring the rapid convergence of GMRES. It has been observed that this strategy provides a good compromise between the convergence of GMRES and the expense of building preconditioners. Moreover, the reliability of the solution is retained even if GMRES fails to converge. In the FANCY code, both the sparse direct solver and the iterative GMRES solver are performed by the sparse matrix solver code (SuperLU version 4.3 [23]), which is complied together with FANCY source code. As shown in Fig. 7, compared with traditional Gaussian elimination dense matrix direct solver, by using current sparse matrix solver model, FANCY is much faster to solve a large scale $N \times N$ sparse matrix for a set of pressure equations. N is the mesh number, which depends on detailed nodalization for the thermal hydraulic system. As a result, FANCY has the capability to simulate transient problems for large scale systems.

3. CODE DEVELOPMENT AND APPLICATION

3.1 Code architecture

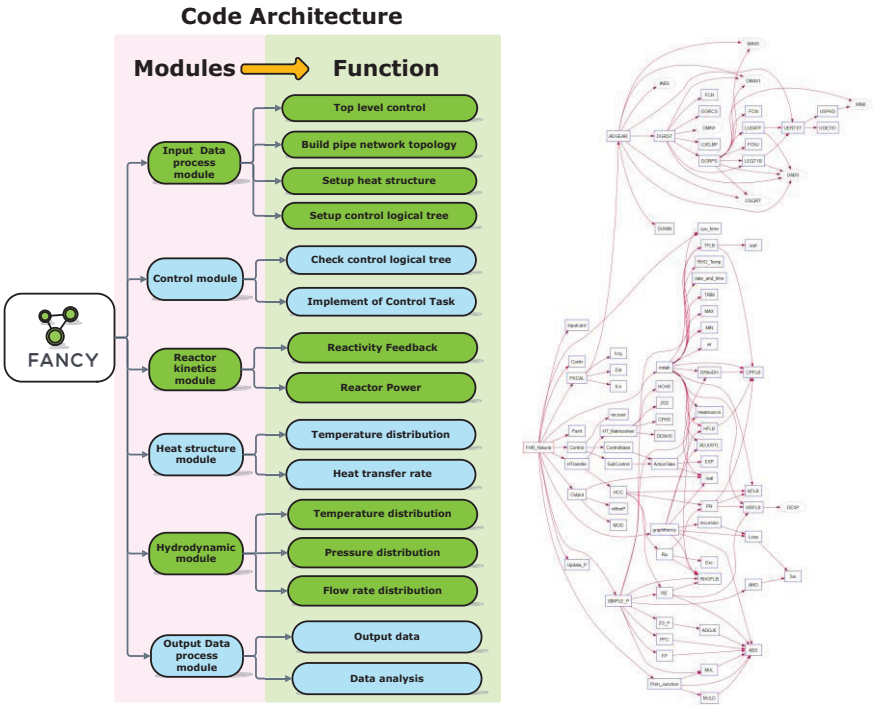

Figure 8. FANCY code architecture (left) and visualization of source code functions relationship (right)

FANCY is a system code based on module technology in Fortran 95, which can compile and execute both on Windows and Linux platforms. All individual models are explicitly coupled in the code structure, as shown in Fig. 8 (left). Although relationships between various functions in the source code are complicated, as shown in Fig. 8 (right), the code has a user-friendly input deck, and the source code does not need to be modified to model specific thermal hydraulic

systems. Furthermore, for advanced applications, each main module has its corresponding set of source code files, which can be modified or updated to add new closure models (e.g. heat transfer coefficient correlations, friction factor correlations, new materials thermal properties, etc.). Each source file has a single purpose, making the whole code easy to maintain and update. Development of the code is under strict version control, using professional version control tools for computer code development. All changes to the code are documented to support future development.

3.2 Nodalization of the Mk1 PB-FHR model

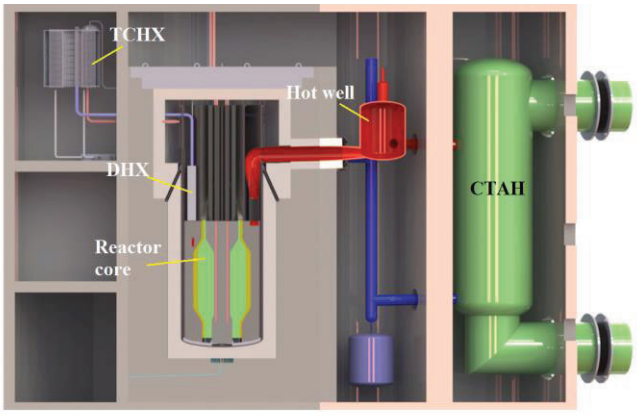

Figure 9. The Mk1 PB-FHR system [24]

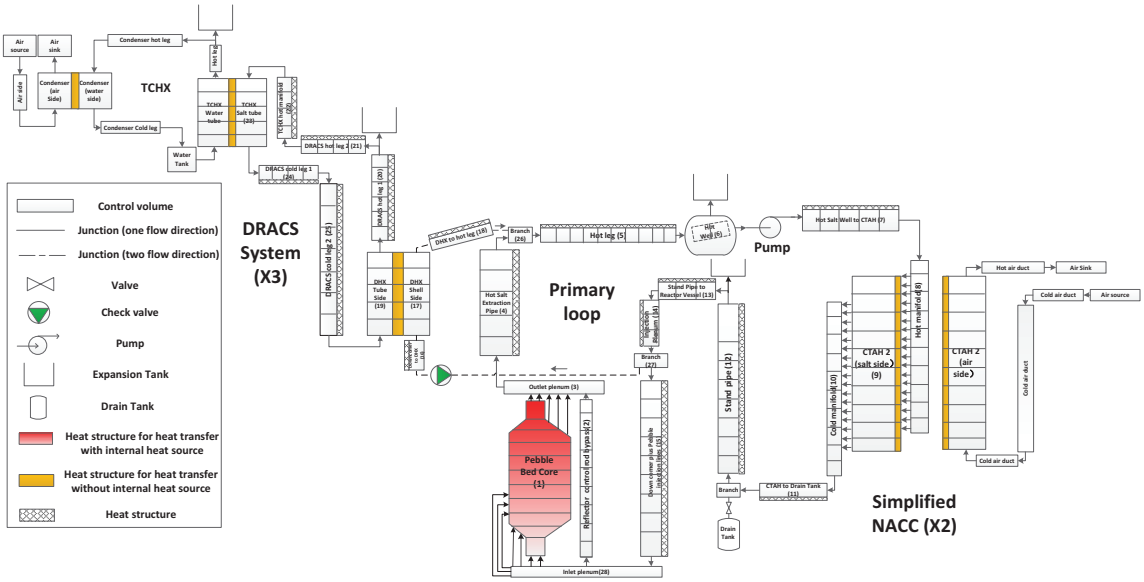

Figure 10. Nodalization of the Mk1 PB-FHR in FANCY, based on equivalent model

Fig. 9 and Fig. 10 show the Mk1 PB-FHR system and the corresponding nodalization diagram, based on an equivalent model of the Mk1 PB-FHR. In the equivalent model, the two coiled tube air heater (CTAH) loops, which transfer heat from the primary loop of the reactor to air in the nuclear air-Brayton combined cycle, are combined into one equivalent loop. Similarly, the three

direct reactor auxiliary cooling system (DRACS) loops, used to passively remove decay heat with natural circulation when the normal shutdown cooling system does not function, are combined into one loop. The reactor core is modeled as a one-dimensional component along the axial direction and radial flow is not modeled. This simplification of the Mk1 PB-FHR thermal hydraulic systems into an equivalent model is the first step in analyzing transient responses of this class of reactors. For V&V purposes, results from this analysis will be compared to experimental data from the CIET facility [5], since CIET scaling was also based on an equivalent model of the PB-FHR. It is worth noting that failure of individual CTAH or DRACS loops cannot be studied using the equivalent model. For example, if loss of force circulation happens in CTAH loop, two CTAH loops will both have pump coast down at the same time. Consequently, it can be regards as conservative safety analysis.

4. SIMULATION RESULTS OF LOFC

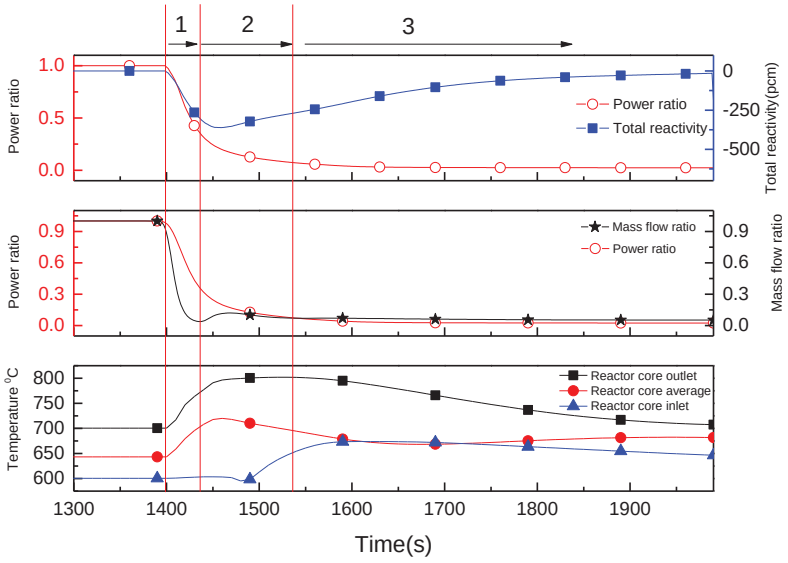

Figure 11. Loss of forced circulation (pump coastdown without scram)

The top graph in Fig. 11 shows the effect of reactivity on power ratio (the ratio of actual power to nominal, normal operation power). The middle graph shows the comparison between the power ratio and the mass flow ratio (the ratio of actual mass flow rate to nominal, normal operation mass flow rate). These competing effects between power and mass flow rate finally affect the whether reactor coolant temperature increase or not, as shown in the bottom graph. The time scales of the three graphs are linked to illustrate the underlying relationship between reactor power, reactivity feedback, temperatures and mass flow rate. With the help of a PI controller, pump head is adjusted automatically to make the system reaches designed steady state before 1400 s. One of the studied accident scenarios is unprotected loss of forced circulation (LOFC). In this case, the reactor power response only depends on the system's negative temperature reactivity feedback. The sequence of events is as follows: pump coastdown happens at 1400 s. Due to lack of pump coastdown data in pre-conceptual design phase of Mk1 PB-FHR, the molten salt reactor experiment (MSRE) pump coast down curve [25, 26] is used temperately. A check valve located in the DHX branch opens approximately 45 s when there is small mass flow reversal in DHX shell side after pump coastdown. The check valve open time is determined by

the static differential pressure of fluid and pressure force needed to open the check valve mechanism that is determined by check valve design.

This LOFC transient can be divided into three main time phases (Fig. 11): during the first phase (before 1400 s – 1450 s), the coolant temperature increases as the reactor core mass flow rate drops, which triggers negative temperature reactivity feedback. Consequently, the reactor power starts to decrease. However, the mass flow rate ratio decreases more rapidly than the power ratio. These competing effects cause the coolant temperature to continue increasing. During the second phase (1450 s – 1530 s), the hydrostatic pressure difference between the inlet and outlet of the check valve increases enough to cause it to open. The natural circulation mass flow rate from the reactor core to the DHX increases. Furthermore, when the power ratio equals the mass flow ratio, 128 s after the LOFC happens, the core outlet coolant temperature reaches its peak temperature. As the DHX outlet temperature increases, the core inlet temperature increases significantly. During the third phase (1530 s – end), the power ratio continues to decrease with negative reactivity feedback, and the increase in heat transfer from the shell side of the DHX to the DRACS loop causes the DHX shell side outlet temperature and the reactor core inlet temperature to drop. Natural circulation from the core to the DHX starts to reach quasi-steady state and the mass flow ratio is larger than the power ratio, causing the coolant temperature to further decrease. The decay heat from actinides, fission products and activation products is then the dominant heat source in the reactor core at this phases and the DRACS system works to extract the decay power.

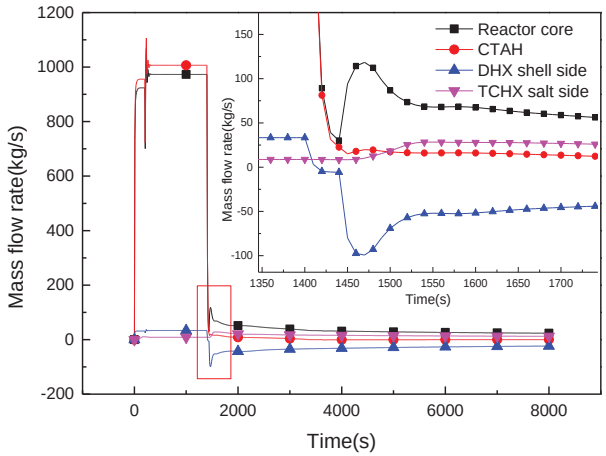

Figure 12. Coolant mass flow rate distribution during LOFC

As shown in Fig.12, from 200 s to 400 s, the system reaches steady state by using a PI control algorithm. 100% mass flow rate goes through the CTAH, 96.6% goes through the core and 3.3% goes through the DHX shell side, transferring heat to the DRACS loop to prevent the flibe in the DRACS loop from freezing. As a result, the DRACS loop has a minor natural circulation flow (9 kg/s) in normal operation. Additionally, there is a 7% bypass flow in the reactor core, through graphite reflectors, control rod insertion channels and injection lines. When pump coastdown happens without check valve open, the total system mass flow rate is at 30 kg/s, which is derived from small natural circulation both from reactor core to CTAH and reactor core to DHX.

Specifically, 100% of this flow goes through the reactor core, 75% goes through the CTAH and 25% goes through the DHX. The flow rate direction reverses in the DHX because during natural circulation operation, the flow direction is from the top inlet to the bottom outlet of the DHX shell side. The check valve opens 45 s into the LOFC transient and the initial natural circulation driving force causes the flow rate in the DHX shell side and the reactor core to increase dramatically. 84% of the total system flow goes through the DHX and 16% goes through the CTAH. The reactor power ratio is 0.16. As heat transfer from the DHX shell side to tube side increases, the natural circulation flow rate increases gradually in the DRACS loop (TCHX mass flow rate in Fig.12). At 3600 s, the system reaches long term steady state conditions. The power ratio is 0.15 and the flow rate in the CTAH is negligible (0.017 kg/s). Therefore, decay heat is mainly extracted by the DRACS system.

5. CONCLUSION

The mathematical model and numerical discretization used in the development of the FANCY system analysis code have been described. FANCY is specifically designed for FHRs with clear modular structure to be maintained and updated, since it is easy to add new heat transfer model as well as hydraulic models from detailed separate effect test in the future. This code has user-friendly input deck to model complicated thermal hydraulics system, which is based on object-oriented concept. FANCY code employs state of the art faster sparse matrix solver to make it has the capability to model large-scale thermal hydraulic system problem. Besides this code can model sequence of events, which is import for safety as well as risk analysis for license of new concept reactor. Detailed code-to-code comparisons and validation are performed in a companion paper from UCB [27]. Accident transients (LOFC) relevant to the Mk1 PB-FHR design were analyzed. The analysis was performed based on an equivalent model, yielding conservative results. The passive mechanisms in the design of the Mk1 PB-FHR guarantee reactor safety during accident transients.

ACKNOWLEDGMENTS

The authors thank Xiaoye S. Li for helpful discussions.
Financial support for Zhangpeng Guo is provided by the China Scholarship Council (CSC), the National Natural Science Foundation of China (NSFC) (Grant No. 91326201). U.S. Department of Energy Office of Nuclear Energy's Nuclear Energy University Programs is gratefully acknowledged for providing funding support for this work.

ACRONYMS AND ABBREVIATIONS

FHR: Fluoride-salt-cooled, high-temperature reactor
CV: control volume
DHX:DRACS heat exchanger
DRACS: Direct reactor auxiliary cooling system
CTAH: Coiled tube air heater
TCHX: Thermosyphon-cooled heat exchanger (in DRACS)
NACC: Nuclear air-Brayton combined cycle

REFERENCES

1. Scarlat, R.O., et al., " Design and licensing strategies for the fluoride-salt-cooled, high-temperature reactor (FHR) technology,"*Progress in Nuclear Energy*, 77, pp. 406–420 (2014).
2. Bardet, P.M. and P.F. Peterson, " Options for scaled experiments for high temperature liquid salt and helium fluid mechanics and convective heat transfer,*" Nuclear Technology*, **163**(3), pp. 344–357 (2008).
3. Peterson, P.F., et al. " Technical Description of the Mark 1 Pebble-Bed Fluoride-Salt-Cooled High-Temperature Reactor (PB-FHR) Power Plant," Technical Report ,University of California, Berkeley (2014).
4. Guo, Z., et al. "Verification and Validation of a Natural Circulation Loop Model for FHRs," *Advances in Thermal Hydraulics (ATH '14)*, Reno, Nevada, June 15–19 , pp.227-246 (2014).
5. Bickel, J.E., N. Zweibaum, and P.F. Peterson. "Design, Fabrication and Startup Testing in the Compact Integral Effects Test (CIET 1.0) Facility in Support of Fluoride-Salt-Cooled, High-Temperature Reactor Technology," University of California, Berkeley (2014).
6. Huddar, L. and P.F. Peterson. "Separate Effects Tests in Support of Heat Transfer Characterization in Fluoride-Salt-Cooled High Temperature Reactors," Technical Report , University of California, Berkeley (2014).
7. N. Zweibaum, Z.G., L. R. Huddar and P. F. Peterson. "Validation of best estimate models for fluoride-salt-cooled, high-temperature reactors using data from the compact integral effects test (CIET 1.0) facility," *The 16th International Topical Meeting on Nuclear Reactor Thermal Hydraulics (NURETH-16)* (2015).
8. Patankar, S.V., "*Numerical Heat Transfer and Fluid Flow*," pp.180-120 ,McGraw-Hill ,USA (1980).
9. Deo, N., "*Graph theory with applications to engineering and computer science*," Prentice-Hall,Inc., USA (2004).
10. Bondy, J.A. and U.S.R. Murty, "*Graph theory with applications*," pp.1-21,Macmillan London,USA (1976).
11. Wang, Y., H.-W. Ge, and R.D. Reitz. "Validation of mesh-and time step-independent spray models for multi-dimensional engine CFD simulation,"SAE Technical Paper,USA (2010).
12. Thermal hydraulics group. "Temperature -Dependent Thermophysical Properties for Fluoride Salts and Simulant Fluids," Technical Report , University of California, Berkeley,USA (2013).
13. IAEA GROUP, I. "After heat Removal for Gas Cooled Reactors Under Accident Conditions," Technical Report ,International Atomic Energy Agency,Vienna, Austria (2001).
14. Cho, N.Z., H. Yu, and J.W. Kim, "Two-temperature homogenized model for steady-state and transient thermal analyses of a pebble with distributed fuel particles*," Annals of nuclear energy*, **36**(4), pp. 448-457(2009).
15. Ergun, S., "Fluid flow through packed columns,"*Chem. Eng. Prog* ,**48**(89), pp.1179-1184 (1952).
16. Sellars, J.R., M. Tribus, and J. Klein. "Heat transfer to laminar flow in a round tube or flat conduit: the Graetz probem extended," US Air Force Technical Report, USA (1954).

17. Churchill, S.W. and H.H.S. Chu, "Correlating equations for laminar and turbulent free convection from a vertical plate," *International Journal of Heat and Mass Transfer*, **18**(11), pp. 1323-1329(1975).
18. Dittus, F. and L. Boelter, "Heat transfer in automobile radiators of the tubular type," *International Communications in Heat and Mass Transfer*, **12**(1), pp. 3-22(1985).
19. Nield, D.A. and A. Bejan, "*Convection in porous media*", springer,USA (2006).
20. Cisneros Jr, A.T., "Pebble Bed Reactors Design Optimization Methods and their Application to the Pebble Bed Fluoride Salt Cooled High Temperature Reactor (PB-FHR)," Ph.D. Dissertation ,University of California, Berkeley (2013).
21. Saad, Y. and M.H. Schultz, "GMRES: A generalized minimal residual algorithm for solving nonsymmetric linear systems," *SIAM Journal on scientific and statistical computing*. **7**(3), pp. 856-869(1986).
22. Demmel, J.W., et al., "A supernodal approach to sparse partial pivoting," *SIAM Journal on Matrix Analysis and Applications*, **20**(3), pp. 720-755(1999).
23. Li, X.S., et al. "SuperLU users' guide," Available from: http://crd-legacy.lbl.gov/~xiaoye/SuperLU/ (2011).
24. Krumwiede, D.L., et al. "Technical Description of the Mark -1 Pebble-Bed Fluoride-Salt-Cooled High-Temperature Reactor (PB-FHR) Power Plant," Technical Report ,University of California, Berkeley,USA,(2014)
25. Pince, B.E., et al. "Zero-power physics experiment on the molten-salt reactor experiment ," Technical Report,ORNL-4233 ,USA(1968).
26. Guo, Z., et al., "Simulations of unprotected loss of heat sink and combination of events accidents for a molten salt reactor," *Annals of Nuclear Energy*, **53**, pp. 309-319 (2013).
27. Zweibaum, N., et al., "Phenomenology, methods and experimental program for fluoride-salt-cooled, high-temperature reactors (FHRs)," *Progress in Nuclear Energy*, **77**,pp.390-405(2014).